On a new numerical analysis of the Hall effect on MHD flow and heat transfer over an unsteady stretching permeable surface in the presence of thermal radiation and heat source/sink

Stanford Shateyi[1*] and Gerald T Marewo[2]

*Correspondence:
stanford.shateyi@univen.ac.za
[1] Department of Mathematics,
University of Venda, Private Bag
X5050, Thohoyandou, 0950, South
Africa
Full list of author information is
available at the end of the article

Abstract

This paper employs a computational iterative approach known as the spectral local linearization method (SLLM) to analyze the Hall effect on MHD flow and heat transfer over an unsteady stretching permeable surface in the presence of thermal radiation and heat source/sink. To demonstrate the reliability of our proposed method, we made comparison with the Matlab *bvp4c* routine technique, and an excellent agreement was observed. The governing partial differential equations are transformed into a system of ordinary differential equations by using suitable similarity transformations. The results are obtained for velocity, temperature, skin friction and the Nusselt number.
MSC: 65PXX; 76-XX

Keywords: spectral local linearization method; Hall effect; thermal radiation; unsteady stretching surface; heat source/sink

1 Introduction

Theoretical studies of magnetohydrodynamic flow and heat transfer over stretching surfaces have received great attention by virtue of their numerous applications in the fields of metallurgy and chemical engineering. Such applications include geothermal reservoirs, wire and fiber coating, food stuff processing, reactor fluidization, enhanced oil recovery, packed bed catalytic reactors and cooling of nuclear reactors. The primary aim in extrusion is to maintain the quality of the surface of the extricate. When the magnetic strength is strong, Hall currents cannot be neglected. In an ionized gas where the density is low and/or the magnetic field is very strong, the conductivity normal to the magnetic field is reduced due to the free spiraling of electrons and ions about the magnetic lines of force before suffering collisions, and a current is induced in a direction normal to both electric and magnetic fields. Due to Hall currents, the electrical conductivity of the fluid becomes anisotropic and this causes the secondary flow. The Hall effect is important when the Hall parameter, which is the ratio between the electron-cyclotron frequency and the electron-atom-collision frequency, is high. Hall currents are of great importance in many

astrophysical problems, Hall accelerators, Hall sensors and flows of plasma in MHD power generators.

Examples of such studies include Sakiadis [1, 2] who did pioneering work on boundary layer flow on a continuously moving surface. Shateyi and Motsa [3] carried out a numerical analysis of the problem of magnetohydrodynamic boundary layer flow, heat and mass transfer rates on steady two-dimensional flow of an electrically conducting fluid over a stretching sheet embedded in a non-Darcy porous medium in the presence of thermal radiation and viscous dissipation. Shateyi [4] investigated thermal radiation and buoyancy effects on heat and mass transfer over a semi-infinite stretching surface with suction and blowing. Singh *et al.* [5] investigated two-dimensional unsteady flow of a viscous incompressible fluid about a stagnation point on a permeable stretching sheet. Shateyi and Motsa [6] numerically investigated the unsteady heat, mass and fluid transfer over a horizontal stretching sheet. More recently, Shateyi and Marewo [7] studied the magnetohydrodynamic boundary layer flow with heat and mass transfer of an UCM fluid over a stretching sheet in the presence of viscous dissipation and thermal radiation. Jhankal [8] considered the problem of unsteady boundary layer and heat transfer over a stretching surface in the presence of a transverse magnetic field.

Pal and Mondal [9] presented a model to study the effects of temperature-dependent viscosity and variable conductivity on mixed convective diffusion of species over a stretching sheet. When the conducting fluid is an ionized gas, and the strength of the applied magnetic field is large, the conductivity normal to the magnetic field is reduced due to the free spiraling of electrons and ions about the magnetic lines of force before collisions occur and a current is induced in a direction normal to both electric and magnetic fields. This phenomenon is known as the Hall effect or Hall current. The conductivity of the fluid is anisotropic and the effect of Hall current cannot be neglected when the medium is rarefied or if a strong magnetic field is present. The study of MHD viscous flows with Hall current has important applications in problems of Hall accelerators and sensors as well as flight magnetohydrodynamics. Pop and Watanabe [10] presented the problem of free convection flow of a conducting fluid which is permeated by a transverse magnetic field and the Hall effect is taken into account. Abd El-Aziz [11] investigated the effect of Hall currents on the flow and heat transfer of an electrically conducting fluid over an unsteady stretching surface in the presence of a strong magnetic field.

Shateyi and Motsa [12] numerically analyzed variable viscosity on magnetohydrodynamic fluid flow and heat transfer over an unsteady stretching surface with the Hall effect. Pal [13] studied the influence of Hall current and thermal radiation on flow and heat transfer characteristics in a viscous fluid over an unsteady stretching permeable surface. Zaman [14] considered the effects of Hall current on the flow of an incompressible, unsteady, viscous, MHD fluid with slip conditions. Lastly, Ali *et al.* [15] investigated heat and mass transfer of a steady flow of an incompressible electrically conducting fluid due to stretching plate under the influence of an applied uniform magnetic field and the effects of Hall current.

Governing equations modeling MHD flow and heat transfer over stretching surfaces are highly nonlinear, thereby exact solutions are impossible to obtain. Therefore, numerical solutions have always been developed and modified as a bid of getting more accurate and stable solutions. The current study seeks to investigate the Hall effect on MHD flow and heat transfer over an unsteady stretching permeable surface in the presence of thermal ra-

diation and heat source/sink. We propose to numerically solve the present problem using a recently developed iterative method known as the spectral local linearization method (SLLM), Motsa [16]. The SLLM approach is based on transforming a nonlinear ordinary differential equation into an iterative scheme. The iterative scheme is then blended with the Chebyshev spectral method [17]. A similar approach to our current proposed method can be found in Motsa and Shateyi [18, 19] and Motsa *et al.* [20].

2 Mathematical formulation

We consider an unsteady two-dimensional laminar MHD boundary layer flow and heat transfer of an incompressible, viscous and electrically conducting fluid over a continuously moving stretching permeable surface. We take the x-axis along the stretching surface in the direction of the motion, and the y-axis is perpendicular to the sheet in the outward direction and the z-axis is transverse to the xy-plane. The flow is subjected to a transverse magnetic field of strength B_0 and the Hall current is taken into account in this study. The effects of the Hall current give rise to the Lorentz force in the z-direction, which induces a cross flow in this direction. We assume that there is no variation of flow and heat transfer quantities in the z-direction. The temperature at the sheet is maintained at a prescribed constant T_w. The flow is generated due to a stretching sheet which is caused by simultaneously applying two equal but opposite forces. The velocity is assumed to be proportional to the distance from the origin. Under these assumptions, together with the usual boundary layer approximations, the dimensional governing equations of continuity, momentum and energy in the presence of a strong magnetic field, heat source and thermal radiation become as follows:

$$\frac{\partial u}{\partial x} + \frac{\partial v}{\partial y} = 0, \tag{1}$$

$$\frac{\partial u}{\partial t} + u\frac{\partial u}{\partial x} + v\frac{\partial u}{\partial y} = \nu\frac{\partial^2 u}{\partial y^2} - \frac{\sigma B^2}{\rho(1+m^2)}(u + mw), \tag{2}$$

$$\frac{\partial w}{\partial t} + u\frac{\partial w}{\partial x} + v\frac{\partial w}{\partial y} = \nu\frac{\partial^2 w}{\partial y^2} - \frac{\sigma B^2}{\rho(1+m^2)}(mu - w), \tag{3}$$

$$\frac{\partial T}{\partial t} + u\frac{\partial T}{\partial x} + v\frac{\partial T}{\partial y} = \alpha\frac{\partial^2 T}{\partial y^2} - \frac{1}{\rho c_p}\frac{\partial q_r}{\partial y} + \frac{Q}{\rho c_p}(T - T_\infty). \tag{4}$$

The associated boundary conditions to the current problem are the following:

$$u = U_w(x,t), \qquad v = V_w, \qquad T = T_w(x,t) \quad \text{at } y = 0,$$

$$u \to 0, \qquad w \to 0, \qquad T \to T_\infty \quad \text{as } y \to \infty, \tag{5}$$

where u, v and w are the velocity components along x, y and z directions, respectively, and t is the time. T is the temperature within the fluid, c_p is the specific heat at constant pressure, α is the thermal diffusivity, ν is the kinematic viscosity of the fluid density, $T_w(x,t)$ is the temperature on the stretching surface, T_∞ is the ambient temperature with $T_w > T_\infty$. We have $V_w = -(\nu U_w/x)^{1/2}f(0)$ representing the mass transfer at the surface with $V_w > 0$ for injection and $V_w < 0$ for suction. We also have $U_w(x,t) = ax/(1 - ct)$, where a (stretching rate) and c are positive constants, with $ct < 1$. It is noted that the stretching rate $a/(1 -$

ct) increases with time since $a > 0$. The surface temperature of the sheet varies with the distance x from the origin and time t and takes the form

$$T_w(x,t) = T_\infty + \frac{b^2 x}{2\nu(1-ct)^{3/2}}, \tag{6}$$

where b is a constant with $b \geq 0$.

We must remark that the particular forms of U_w and $T_w(x,t)$ have been specifically chosen in order to come up with similarity transformations which then transform the governing partial differential equations into a set of nonlinear ordinary differential equations.

Following Ishak *et al.* [21], we introduce the following dimensionless functions f and θ, and the similarity variable η,

$$\eta = \left(\frac{b}{\nu(1-ct)}\right)^{\frac{1}{2}} y, \qquad \psi(x,y,t) = \left(\frac{\nu b}{1-ct}\right)^{\frac{1}{2}} x f(\eta),$$

$$T(x,y,t) = T_\infty + \frac{b^2 x}{2\nu(1-ct)^{\frac{3}{2}}}\theta(\eta), \qquad B^2 = \frac{B_0^2}{(1-ct)}. \tag{7}$$

By using the Rosseland approximation, the radiative heat flux is given by

$$q_r = -\frac{4\sigma^*}{3K^*}\frac{\partial T^4}{\partial y}, \tag{8}$$

where σ^* and K^* are, respectively, the Stephan-Boltzman constant and the mean absorption coefficient. Assume that the temperature differences within the flow are small such that T^4 can be expressed as a linear function. Expanding T^4 in a Taylor series about T_∞ and neglecting higher order terms, we get

$$T^4 \cong 4T_\infty T - 3T_\infty^4. \tag{9}$$

By using the above transformations, the governing partial differential equations are transformed into a system of non-dimensional nonlinear and coupled ordinary differential equations as follows:

$$f''' + ff'' - f'^2 - A\left(f' + \frac{1}{2}\eta f''\right) - \frac{M}{1+m^2}(f' + mg) = 0, \tag{10}$$

$$g'' + fg' - f'g - A\left(g + \frac{1}{2}\eta g'\right) - \frac{M}{1+m^2}(mf' - g) = 0, \tag{11}$$

$$\left(1 + \frac{4}{3}R\right)\theta'' + Pr(f\theta' - 2f'\theta) - Pr\frac{A}{2}(3\theta + \eta\theta') + \delta\theta = 0. \tag{12}$$

Here $M^2 = \sigma B_0^2/\rho a$ is the magnetic parameter, $A = c/a$ is a parameter that measures the unsteadiness, $Pr = \nu/\alpha$ is the Prandtl number, $R = 4\sigma^* T_\infty^3/kK_s$ is the thermal radiation parameter. The boundary conditions are as follows:

$$f(0) = f_w, \qquad f'(0) = 1, \qquad \theta(0) = 1, \qquad g(0) = 0, \tag{13}$$

$$f' \to 0, \qquad \theta \to 0, \qquad g \to 0 \quad \text{as } \eta \to \infty, \tag{14}$$

where $f(0) = f_w$ with $f_w < 0$ or $f_w > 0$ corresponding to injection or suction, respectively. The physical engineering quantities of interest in this problem are the skin friction coefficients in the x- and z-directions and the local Nusselt number, Nu_x which are defined as follows:

$$
\begin{aligned}
C_{fx} &= -\frac{2\mu(\partial u/\partial y)_{y=0}}{\rho U_w^2} = -2Re_x^{-1/2}f''(0),\\
C_{fz} &= \frac{2\mu(\partial w/\partial y)_{y=0}}{\rho U_w^2} = 2Re_x^{-1/2}g'(0),\\
Nu_x &= \frac{xq_w}{\kappa(Tw - T_\infty)},
\end{aligned}
\tag{15}
$$

where $\tau_w = \mu(\frac{\partial u}{\partial y})_{y=0}$ is the wall shear stress, and $q_w = -\kappa(\frac{\partial T}{\partial y})_{y=0}$ is the surface heat flux, where μ and κ are the dynamic viscosity and thermal conductivity, respectively.

3 Method of solution

3.1 Basic idea of the spectral local linearization method (SLLM)

Consider the problem of finding $\mathbf{Z} = [Z_1(\eta), Z_2(\eta), \ldots, Z_m(\eta)]$ that satisfies the system

$$
L_i + N_i = H_i,
\tag{16}
$$

of m differential equations, where $i = 1, 2, \ldots, m$, and each H_i is a function of $\eta \in [a, b]$. Also, L_i and N_i are linear and nonlinear components, respectively.

Basically, the SLLM is an iterative method for solving differential equations such as (16) which begins with an initial approximation $\mathbf{Z}_0$ of $\mathbf{Z}$. Successive application of the SLLM generates approximations $\mathbf{Z}_1, \mathbf{Z}_2, \ldots$, where $\mathbf{Z}_r = [Z_{1,r}, \ldots, Z_{m,r}]$ for each $r = 0, 1, 2, \ldots$. Upon linearizing nonlinear component N_i, differential equation (16) shall be solved numerically using the Chebyshev spectral collocation method [17].

First, let

$$
L_i|_{r+1} + N_i|_{r+1} = H_i
\tag{17}
$$

denote the ith differential equation (16) after the first $r + 1$ iterations of the SLLM. Let $\mathbf{w}_r$ be an n-tuple of $Z_{i,r}$ and its derivatives. If we assume that N_i is a function of $\mathbf{w}_r$ only, then linearization of N_i at $\mathbf{w}_r$ is

$$
N_i|_{r+1} \approx N_i|_{r+1} + \nabla N_i|_r \cdot (\mathbf{w}_{r+1} - \mathbf{w}_r),
\tag{18}
$$

which, upon inserting into equation (17) and re-arranging the result, gives

$$
L|_{r+1} + \nabla N_i|_r \cdot \mathbf{w}_{r+1} = H_i + \nabla N_i|_r \cdot \mathbf{w}_r - N_i|_r.
\tag{19}
$$

Equation (19) shall be solved using the Chebyshev spectral collocation method. For the sake of brevity, we leave out the details of this method. We urge the interested reader to see, for example, [22].

3.2 Solving current problem using the SLLM

If we let $f' = p$, then equations (10)-(12) become

$$p'' + fp' - p^2 - A\left(p + \frac{\eta}{2}p'\right) - \frac{M}{1 + m^2}(p + mg) = 0, \tag{20}$$

$$g'' + fg' - pg - A\left(g + \frac{\eta}{2}g'\right) + \frac{M}{1 + m^2}(mp - g) = 0, \tag{21}$$

$$\left(1 + \frac{4}{3}R\right)\theta'' + Pr(f\theta' - 2p\theta) - Pr\frac{A}{2}(3\theta + \eta\theta') + \delta\theta = 0. \tag{22}$$

Equations (20)-(22) together with the change of variable $f' = p$ may be written as

$$L_1 + N_1 = H_1, \tag{23}$$

$$L_2 + N_2 = H_2, \tag{24}$$

$$L_3 + N_3 = H_3, \tag{25}$$

$$L_4 + N_4 = H_4, \tag{26}$$

where

$$L_1 = f' - p, \qquad N_1 = 0, \qquad H_1 = 0, \tag{27}$$

$$L_2 = p'' - \left(A + \frac{M}{1 + m^2}\right)p - A\frac{\eta}{2}p' - \frac{Mm}{1 + m^2}g,$$

$$N_2(p, p') = fp' - p^2, \qquad H_2 = 0, \tag{28}$$

$$L_3 = g'' - \left(A + \frac{M}{1 + m^2}\right)g - A\frac{\eta}{2}g' + \frac{Mm}{1 + m^2}p,$$

$$N_3(g, g') = fg' - pg, \qquad H_3 = 0, \tag{29}$$

$$L_4 = \left(1 + \frac{4}{3}R\right)\theta'' - PrA\frac{\eta}{2}\theta' + \left(\delta - \frac{3}{2}PrA\right)\theta,$$

$$N_4(\theta, \theta') = Pr(f\theta' - 2p\theta), \qquad H_4 = 0. \tag{30}$$

As an illustration we derive equation (19) when $i = 2$. In this case, equation (19) is

$$L_2|_{r+1} + \frac{\partial N_2}{\partial p}\bigg|_{r+1} p_{r+1} + \frac{\partial N_2}{\partial p'}\bigg|_{r+1} p'_{r+1} = H_2 + \frac{\partial N_2}{\partial p}\bigg|_{r+1} p_r + \frac{\partial N_2}{\partial p'}\bigg|_{r+1} p'_r - N_2|_r, \tag{31}$$

which, upon substituting (28) and simplifying, becomes

$$p''_{r+1} - \left(A + \frac{M}{1 + m^2}\right)p_{r+1} - A\frac{\eta}{2}p'_{r+1} - 2p_r p_{r+1} + f_r p'_{r+1} - \frac{Mm}{1 + m^2}g_{r+1} = -p_r^2. \tag{32}$$

A similar approach for each $i = 1, 3, 4$ yields

$$f'_{r+1} = p_{r+1}, \tag{33}$$

$$g''_{r+1} - A\frac{\eta}{2}g'_{r+1} - \left(A + \frac{M}{1 + m^2}\right)g_{r+1} - p_r g_{r+1} + f_r g'_{r+1} + \frac{Mm}{1 + m^2}p_{r+1} = 0, \tag{34}$$

$$\left(1 + \frac{4}{3}R\right)\theta''_{r+1} - PrA\frac{\eta}{2}\theta'_{r+1} + \left(\delta - \frac{3}{2}PrA\right)\theta_{r+1} - 2Prp_r\theta_{r+1} + Prf_r\theta'_{r+1} = 0. \tag{35}$$

Equations (32)-(35) are subject to the boundary conditions

$$p_{r+1}(0) = 1, \qquad p_{r+1}(\infty) = 0, \tag{36}$$

$$f_{r+1}(0) = f_w, \tag{37}$$

$$g_{r+1}(0) = 0, \qquad g_{r+1}(\infty) = 0, \tag{38}$$

$$\theta_{r+1}(0) = 1, \qquad \theta_{r+1}(\infty) = 0, \tag{39}$$

respectively. Chebyshev differentiation [17] replaces equations (32) through (35) with the discrete form

$$\begin{pmatrix} D & -I & O & O \\ O & A_{11} & A_{12} & O \\ O & A_{21} & A_{22} & O \\ O & O & O & A_3 \end{pmatrix} \begin{pmatrix} \mathbf{f}_{r+1} \\ \mathbf{p}_{r+1} \\ \mathbf{g}_{r+1} \\ \boldsymbol{\Theta}_{r+1} \end{pmatrix} = \begin{pmatrix} \mathbf{0} \\ B_1 \\ B_2 \\ B_3 \end{pmatrix} \tag{40}$$

or equivalently

$$D\mathbf{f}_{r+1} = \mathbf{p}_{r+1}, \tag{41}$$

$$\begin{pmatrix} A_{11} & A_{12} \\ A_{21} & A_{22} \end{pmatrix} \begin{pmatrix} \mathbf{p}_{r+1} \\ \mathbf{g}_{r+1} \end{pmatrix} = \begin{pmatrix} B_1 \\ B_2 \end{pmatrix}, \tag{42}$$

$$A_3\boldsymbol{\Theta}_{r+1} = B_3 \tag{43}$$

subject to the boundary conditions

$$f_{r+1}(\tau_N) = f_w,$$

$$p_{r+1}(\tau_N) = 1, \qquad p_{r+1}(\tau_0) = 0,$$

$$g_{r+1}(\tau_N) = 0, \qquad g_{r+1}(\tau_0) = 0,$$

$$\theta_{r+1}(\tau_N) = 1, \qquad \theta_{r+1}(\tau_0) = 0,$$

where

$$A_{11} = D^2 + \text{diag}\left\{\mathbf{f}_r - A\frac{\eta}{2}\right\}D - 2\,\text{diag}\{\mathbf{p}_r\} - \left(A + \frac{M}{1 + m^2}\right)I,$$

$$A_{12} = -\frac{Mm}{1 + m^2}I, \qquad B_1 = -\mathbf{p}_r^2,$$

$$A_{22} = D^2 + \text{diag}\left\{\mathbf{f}_r - A\frac{\eta}{2}\right\}D - \text{diag}\{\mathbf{p}_r\} - \left(A + \frac{M}{1 + m^2}\right)I,$$

$$A_{21} = \frac{Mm}{1 + m^2}I, \qquad B_2 = \mathbf{0},$$

$$A_3 = \left(1 + \frac{4}{3}R\right)D^2 + Pr\,\text{diag}\left\{\mathbf{f}_r - A\frac{\eta}{2}\right\}D - 2Pr\,\text{diag}\{\mathbf{p}_r\} + \left(\delta - \frac{3}{2}PrA\right)I, \qquad B_3 = \mathbf{0}$$

and O, $\mathbf{0}$ are zero matrices of order $(N + 1) \times (N + 1)$, $(N + 1) \times 1$, respectively. Before we solve linear system (40), we need to apply boundary conditions. This is easier to illustrate using the equivalent form, equations (41)-(43), as follows:

$$
\begin{pmatrix}
 & D & \\
\hline
0 & 0 & \cdots & 1
\end{pmatrix}
\begin{pmatrix}
f_{r+1}(\tau_0) \\
\vdots \\
f_{r+1}(\tau_N)
\end{pmatrix}
=
\begin{pmatrix}
\mathbf{p}_{r+1} \\
\hline
f_w
\end{pmatrix},
$$

$$
\begin{pmatrix}
1 & 0 & \cdots & 0 & 0 & 0 & \cdots & 0 \\
 & A_{11} & & & & A_{12} & & \\
0 & \cdots & 0 & 1 & 0 & \cdots & 0 & 0 \\
0 & 0 & \cdots & 0 & 1 & 0 & \cdots & 0 \\
 & A_{21} & & & & A_{22} & & \\
0 & 0 & \cdots & 0 & 0 & 0 & \cdots & 1
\end{pmatrix}
\begin{pmatrix}
p_{r+1}(\tau_0) \\
\vdots \\
p_{r+1}(\tau_N) \\
g_{r+1}(\tau_0) \\
\vdots \\
g_{r+1}(\tau_N)
\end{pmatrix}
=
\begin{pmatrix}
0 \\
B_1 \\
1 \\
0 \\
B_2 \\
0
\end{pmatrix},
$$

$$
\begin{pmatrix}
1 & 0 & \cdots & 0 \\
 & A_3 & & \\
0 & \cdots & 0 & 1
\end{pmatrix}
\begin{pmatrix}
\theta_{r+1}(\tau_0) \\
\vdots \\
\theta_{r+1}(\tau_N)
\end{pmatrix}
=
\begin{pmatrix}
0 \\
B_3 \\
1
\end{pmatrix}.
$$

We choose initial approximations

$$
f_0(\eta) = f_w + 1 - e^{-\eta},
$$
$$
p_0(\eta) = \theta_0(\eta) = e^{-\eta},
$$
$$
g_0(\eta) = \eta e^{-\eta}
$$

that satisfy boundary conditions (36)-(39) so that the SLLM generates subsequent approximations f_r, p_r, g_r, θ_r for each $r = 1, 2, \ldots$.

4 Results and discussion

The numerical results iteratively generated by the SLLM for the main parameters that have significant effects on the flow properties are presented in this section. All the SLLM results presented in this work were obtained using $N = 50$ collocation points, and we are glad to highlight that convergence was achieved in as few as six iterations. We take the infinity value η_∞ to be 40. The magnetic field is taken quite strong by assigning large values of M to ensure the generation of Hall currents. In order to validate our numerical method, it was compared to MATLAB routine *bvp4c* which is an adaptive Lobatto quadrature iterative scheme.

In Table 1 we present a comparison between the SLLM approximate results and the *bvp4c* results for selected default values of the stretching parameter A. It can be clearly seen from this table that there is an excellent agreement between the results from the two methods. Also Table 1 shows that an increase in the unsteadiness parameter leads to an increase in the skin-friction coefficients in both directions. Also the heat transfer gradient increases as the values of the unsteadiness parameter increase. The negative values of $f''(0)$ mean that the solid surface exerts a drag force on the fluid. This is due to the development

Table 1 Comparison of the SLLM results of $-f''(0)$, $g'(0)$, $-\theta'(0)$ with those obtained by *bvp4c* for different values of the unsteadiness parameter

A	$-f''(0)$		$g'(0)$		$-\theta'(0)$	
	bvp4c	SLLM	bvp4c	SLLM	bvp4c	SLLM
1	2.06334096	2.06334096	0.17551632	0.17551632	0.95973533	0.95973533
2	2.27277685	2.27277685	0.15185421	0.15185421	1.30758931	1.30758931
3	2.46649701	2.46649701	0.13459762	0.13459762	1.54422525	1.54422525

Table 2 Comparison of the SLLM results of $-f''(0)$, $g'(0)$, $-\theta'(0)$ with those obtained by *bvp4c* for different values of the magnetic parameter

M	$-f''(0)$		$g'(0)$		$-\theta'(0)$	
	bvp4c	SLLM	bvp4c	SLLM	bvp4c	SLLM
1	2.06334096	2.06334096	0.17551632	0.17551632	0.51730365	0.51730365
3	2.40059801	2.40059801	0.41757839	0.41757839	0.46087659	0.46087659
5	2.69187810	2.69187810	0.59380491	0.59380491	0.43117279	0.43117279

Table 3 Comparison of the SLLM results of $-f''(0)$, $g'(0)$, $-\theta'(0)$ with those obtained by *bvp4c* for different values of the Hall parameter

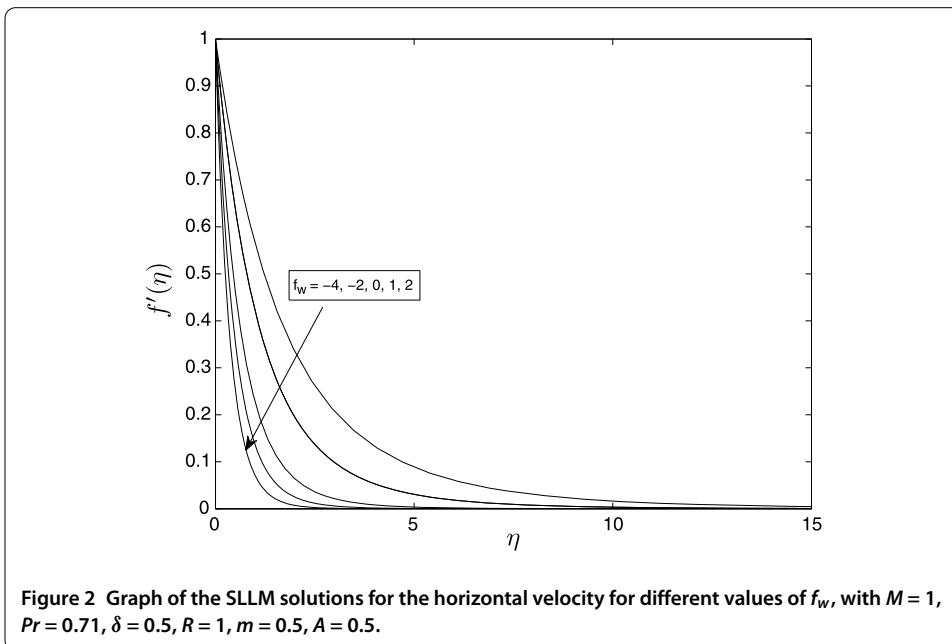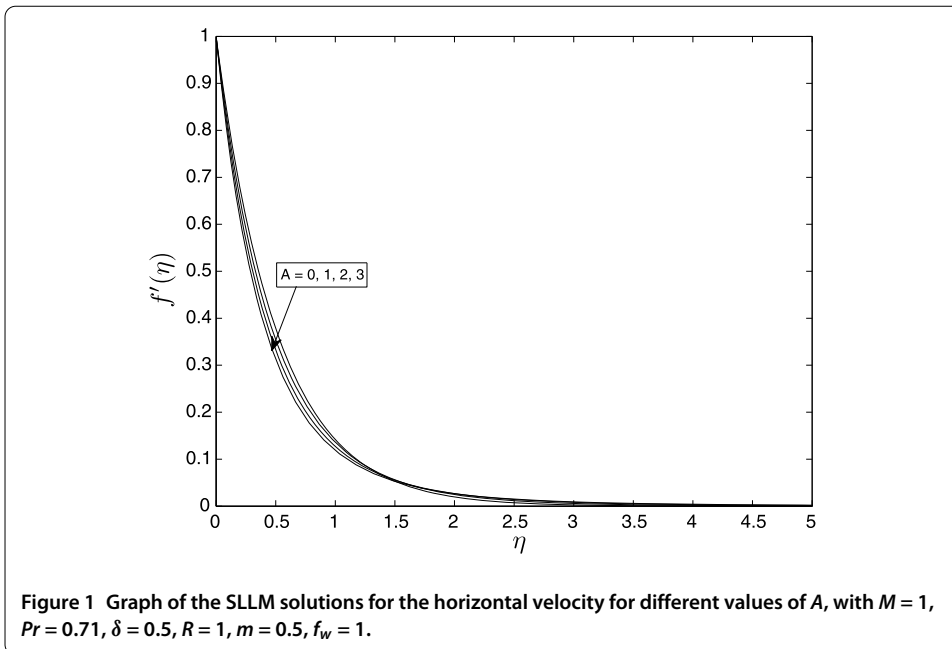| m	$-f''(0)$		$g'(0)$		$-\theta'(0)$	
	bvp4c	SLLM	bvp4c	SLLM	bvp4c	SLLM
0.1	2.20591638	2.20591638	0.03127850	0.03127850	0.49780303	0.49780303
0.5	2.15366831	2.15366831	0.13112526	0.13112526	0.50406091	0.50406091
1.0	2.06334096	2.06334096	0.17551632	0.17551632	0.51730365	0.51730365

of the velocity boundary layer which in the current study is caused solely by the stretching sheet.

In Table 2 we display the effect of the magnetic parameter on the skin friction coefficients and the Nusselt number. The magnetic parameter M represents the significance of the magnetic field on the flow properties. As the magnetic strength increases, the dragging effect is clearly seen by the significant increments in the skin friction. We also observe that increasing the values of the Hartman number leads to the lowering of the values of the Nusselt number. Application of a strong magnetic field reduces the velocity, which in turn increases heat diffusion within the fluid flow. This physically explains why heat transfer at the wall is reduced as M is increased.

Table 3 displays the influence of the Hall current on the skin friction coefficients as well as the Nusselt number. The skin friction coefficient is reduced as the values of the Hall current parameter increase. This explains why the skin friction coefficient in the axial direction decreases. However, in the transverse direction the skin friction increases as the Hall current increases. There is a small effect of the Hall current on heat transfer rate on the stretching surface.

The effect of the unsteadiness parameter A on the axial velocity $f'(\eta)$ is presented in Figure 1. It can be observed from this figure that the axial velocity profiles decrease as A increases. Increasing the unsteadiness parameter A causes the velocity boundary layer thickness to decrease. This in turn may cause delays in transition from laminar to turbulent flows.
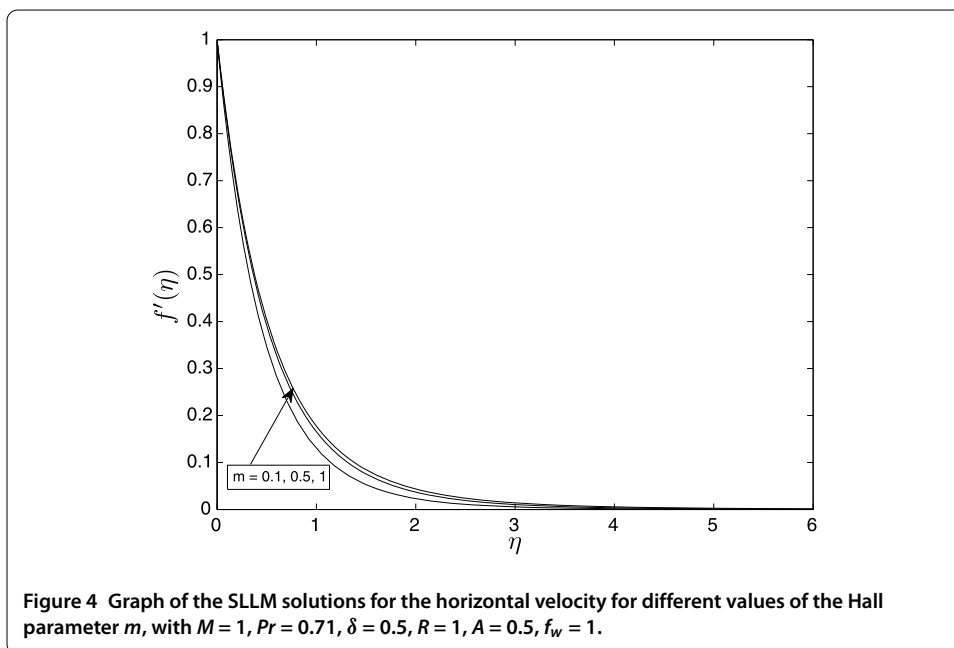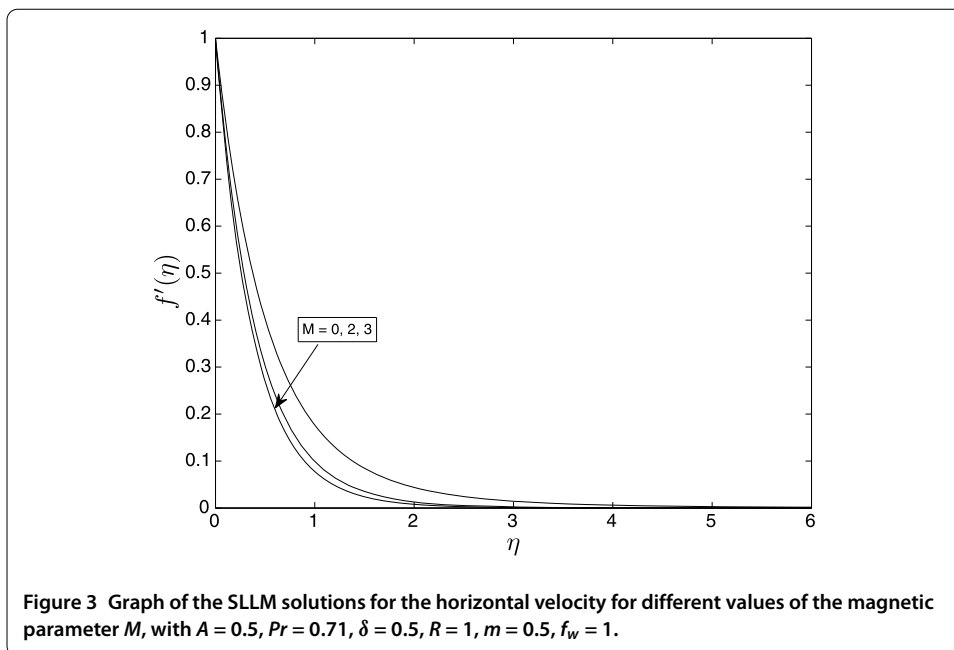
The influence of the suction/injection parameter f_w on the axial velocity is depicted in Figure 2. The axial velocity is significantly influenced by this parameter. The velocity boundary layer is greatly enhanced when fluid is injected ($f_w < 0$) into the flow system thereby increasing the velocity profiles. However, removing fluid from the flow system

Figure 1 Graph of the SLLM solutions for the horizontal velocity for different values of *A*, with *M* = 1, *Pr* = 0.71, δ = 0.5, *R* = 1, *m* = 0.5, f_w = 1.

Figure 2 Graph of the SLLM solutions for the horizontal velocity for different values of f_w, with *M* = 1, *Pr* = 0.71, δ = 0.5, *R* = 1, *m* = 0.5, *A* = 0.5.

through suction, as expected, drastically reduces the velocity profiles as can be clearly seen in Figure 2.
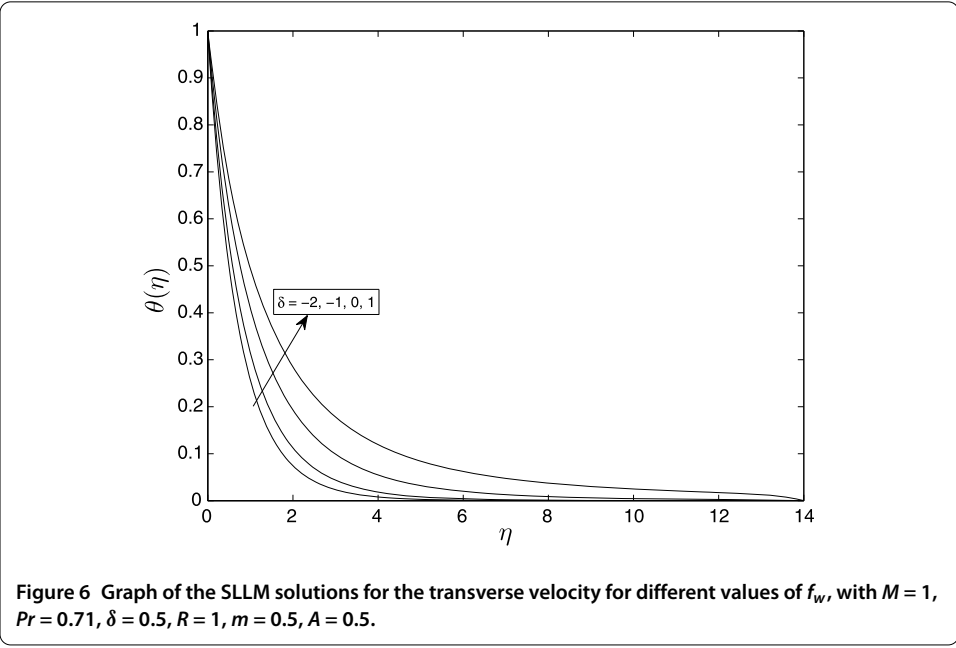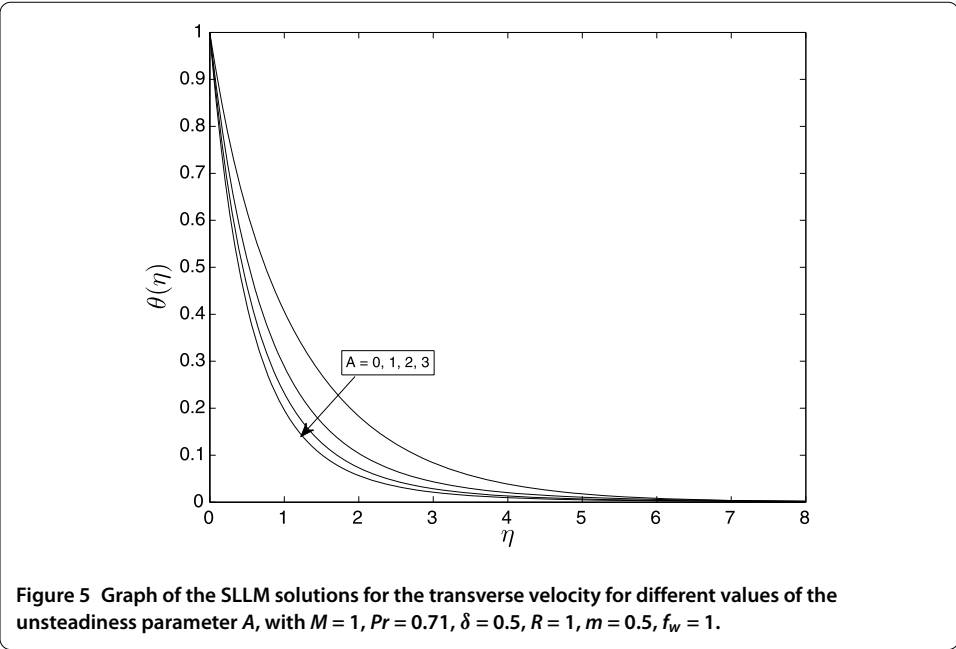
The application of a magnetic field perpendicular to the flow produces a drag force known as the Lorentz force. This force reduces the axial velocity as can be observed in Figure 3. Thus increasing the magnetic strength parameter *M* reduces the velocity boundary layer and thereby reduces the velocity profiles.

The effect of the Hall current parameter *m* on the axial velocity is shown in Figure 4. The velocity is enhanced as the values of *m* increase. However, the axial velocity profiles approach their classical values when the Hall current parameter *m* becomes large ($m > 1.5$)

Figure 3 Graph of the SLLM solutions for the horizontal velocity for different values of the magnetic parameter M, with $A = 0.5$, $Pr = 0.71$, $\delta = 0.5$, $R = 1$, $m = 0.5$, $f_w = 1$.

Figure 4 Graph of the SLLM solutions for the horizontal velocity for different values of the Hall parameter m, with $M = 1$, $Pr = 0.71$, $\delta = 0.5$, $R = 1$, $A = 0.5$, $f_w = 1$.
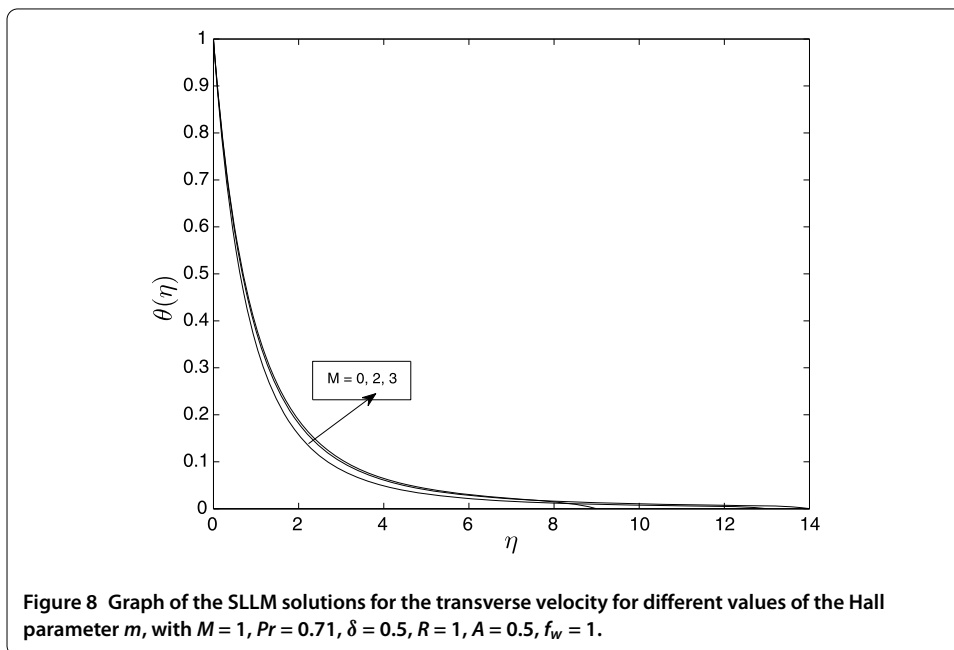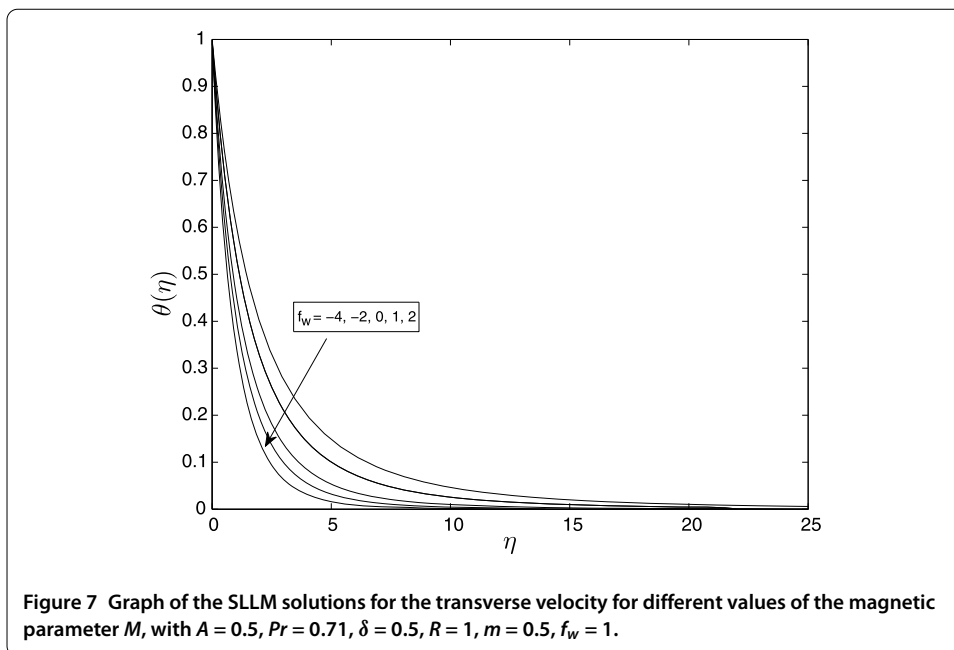
in our current study. Any further increase of the Hall current would make the magnetic effect insignificant.

Figure 5 displays the effect of the unsteadiness parameter on the transverse velocity profiles. This parameter has very significant influence on the transverse velocity. It can clearly be seen from this figure that the effect of increasing the unsteadiness parameter A is to greatly reduce the transverse velocity $g(\eta)$ near the plate. In Figure 6, we display the influence of the injection/suction parameter on the transverse velocity. Injecting/blowing fluid into the flow system causes the transverse velocity profiles to significantly increase, whereas suction, as expected, reduces the transverse velocity distribution.

Figure 5 Graph of the SLLM solutions for the transverse velocity for different values of the unsteadiness parameter A, with $M = 1$, $Pr = 0.71$, $\delta = 0.5$, $R = 1$, $m = 0.5$, $f_w = 1$.

Figure 6 Graph of the SLLM solutions for the transverse velocity for different values of f_w, with $M = 1$, $Pr = 0.71$, $\delta = 0.5$, $R = 1$, $m = 0.5$, $A = 0.5$.

The influence of the magnetic parameter M on the transverse velocity is depicted in Figure 7. One can clearly observe in this figure that the magnetic parameter M has a very significant effect on the transverse velocity profiles. An increase in the values of M leads to a huge increase in the values of the transverse velocity due to the Lorentz force which acts in the direction hence tends to accelerate the fluid flow in the traverse direction.
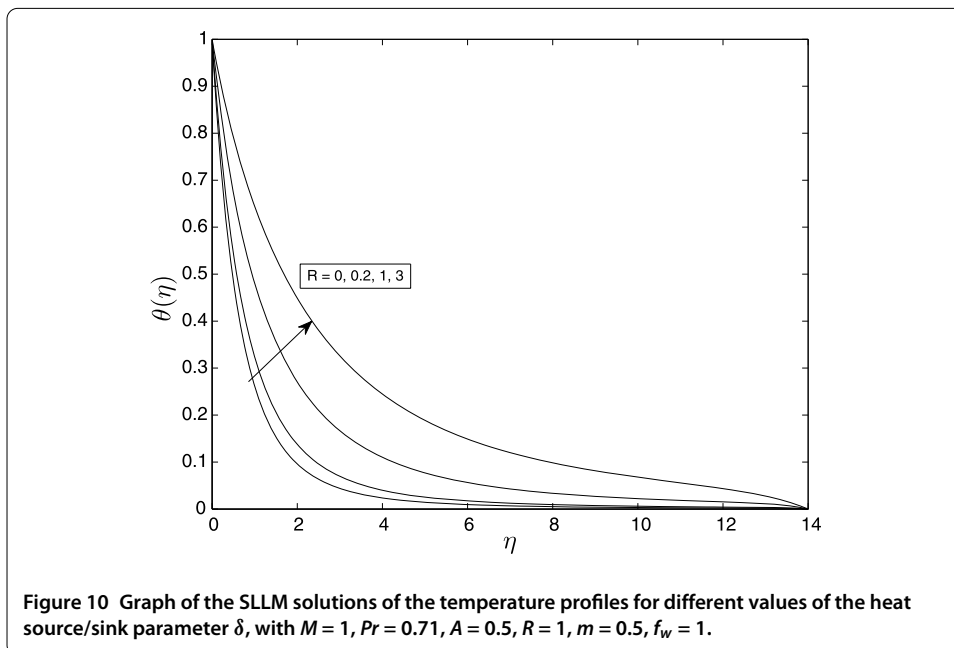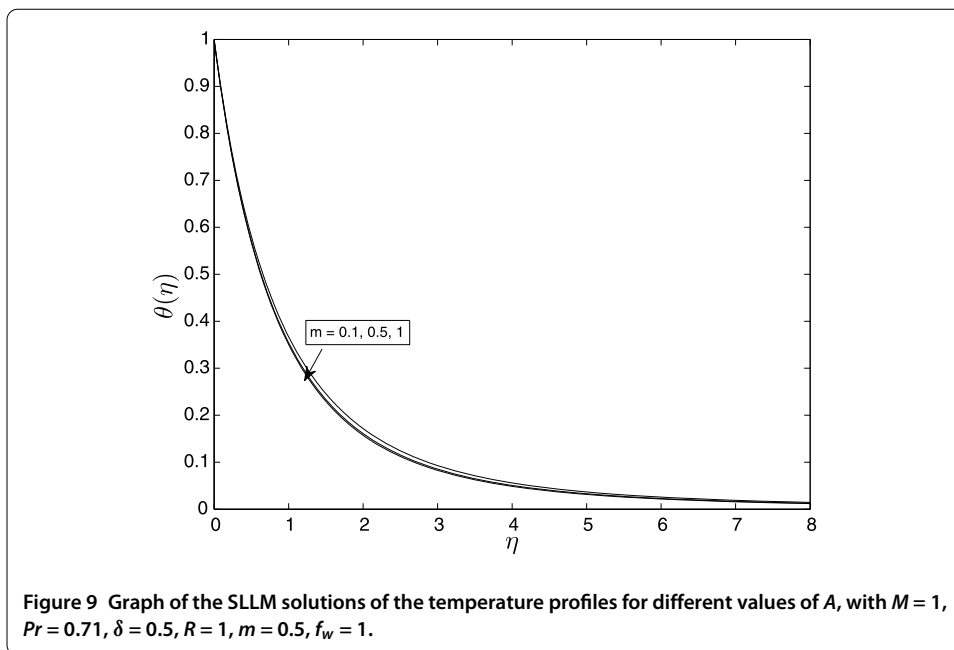
The effect of the Hall current parameter on the transverse velocity is displayed in Figure 8. Increasing the values of m causes the transverse velocity to rapidly increase. Figure 9 shows the effect of the unsteadiness parameter A on the temperature profiles. Increasing

Figure 7 Graph of the SLLM solutions for the transverse velocity for different values of the magnetic parameter *M*, with *A* = 0.5, *Pr* = 0.71, δ = 0.5, *R* = 1, *m* = 0.5, f_w = 1.

Figure 8 Graph of the SLLM solutions for the transverse velocity for different values of the Hall parameter *m*, with *M* = 1, *Pr* = 0.71, δ = 0.5, *R* = 1, *A* = 0.5, f_w = 1.

the values of A reduces the thermal boundary layer thickness thus reducing the fluid temperature distribution.

In Figure 10 we have the effect of the heat source/sink parameter δ on the temperature profiles. As expected, it is observed in this figure that the temperature in the boundary layer increases with increasing values of δ. The heat absorption due to a uniform sink ($\delta < 0$) leads to the reduction of the thermal boundary layer thickness, whereas this layer increases significantly with increases in $\delta > 0$.
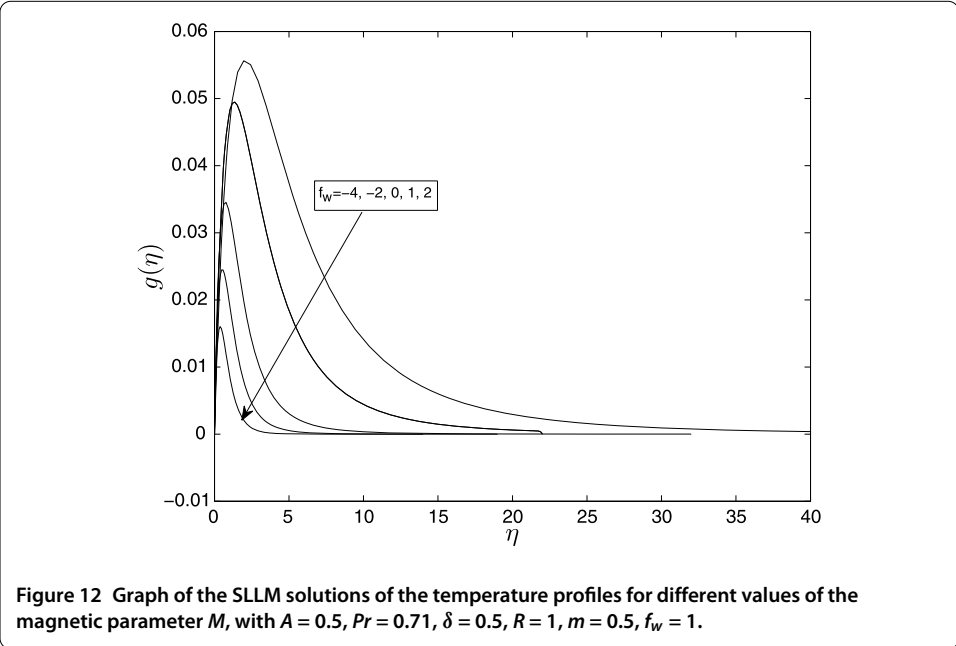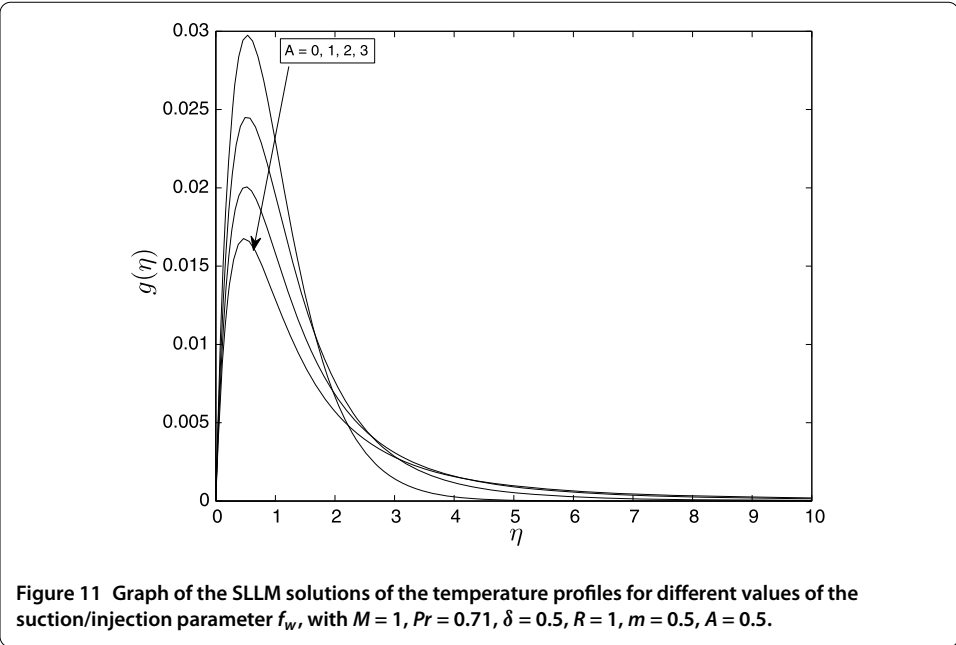
Figure 11 shows the effect of injection/suction on the temperature profiles. Injecting fluid into the flow system causes enhancement of the thermal boundary layer thickness.

Figure 9 Graph of the SLLM solutions of the temperature profiles for different values of *A*, with *M* = 1, *Pr* = 0.71, δ = 0.5, *R* = 1, *m* = 0.5, f_w = 1.

Figure 10 Graph of the SLLM solutions of the temperature profiles for different values of the heat source/sink parameter δ, with *M* = 1, *Pr* = 0.71, *A* = 0.5, *R* = 1, *m* = 0.5, f_w = 1.

This in turn causes the temperature distribution in the flow system to greatly increase. On the other hand, suction reduces the thermal boundary layer thickness.

Figure 12 shows that the thermal boundary layer becomes thicker when the values of the magnetic parameter are increased. Application of the magnetic field gives rise to a resistive-type force which slows down the motion of the fluid and in turn increases the thermal boundary layer, hence increasing the temperature of the fluid.
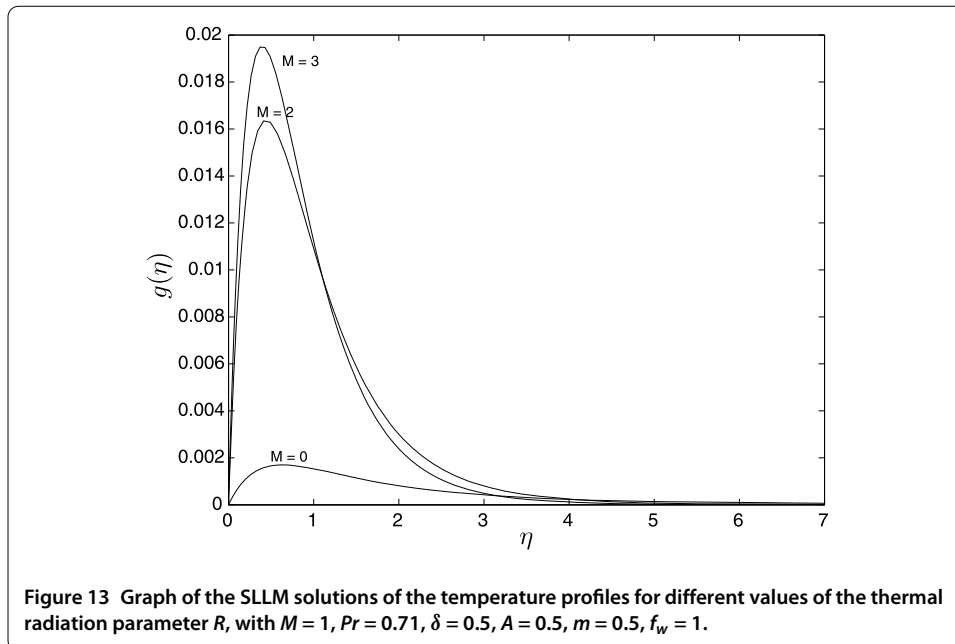
Figure 13 is plotted to depict the influence of the thermal radiation parameter *R* on the temperature profiles. We clearly observe that the temperature in the boundary layer increases with increasing values of the thermal radiation parameter. This is due to the fact

Figure 11 Graph of the SLLM solutions of the temperature profiles for different values of the suction/injection parameter f_w, with $M = 1$, $Pr = 0.71$, $\delta = 0.5$, $R = 1$, $m = 0.5$, $A = 0.5$.

Figure 12 Graph of the SLLM solutions of the temperature profiles for different values of the magnetic parameter M, with $A = 0.5$, $Pr = 0.71$, $\delta = 0.5$, $R = 1$, $m = 0.5$, $f_w = 1$.

that the divergence of the radiative heat flux increases as the Rosseland radiative absorption K^* decreases, which in turn increases the rate of radiative heat transfer to the fluid. Thus the presence of thermal radiation enhances thermal state of the fluid causing its temperature to significantly increase.

5 Conclusion

The present work analyzed MHD unsteady flow and heat transfer of an electrically conducting fluid over a stretching sheet in the presence of thermal radiation and the Hall effect. Much attention was given to trying to investigate how the velocity field, skin friction,

Figure 13 Graph of the SLLM solutions of the temperature profiles for different values of the thermal radiation parameter *R*, with *M* = 1, *Pr* = 0.71, *δ* = 0.5, *A* = 0.5, *m* = 0.5, f_w = 1.

temperature distribution and heat transfer are influenced by the parameters of importance in this study. The governing partial differential equations are transformed into a system of nonlinear ordinary differential equations by using suitable similarity variables. The resultant system of nonlinear ordinary differential equations is solved numerically by a recently developed technique known as the spectral local linearization method. The accuracy of the SLLM is validated against the MATLAB in-built *bvp*4*c* routine for solving boundary value problems. The following conclusions were drawn in our investigation.

- An excellent agreement was observed between our results and those obtained using the *bvp*4*c* routine technique giving confidence to our present results.
- The unsteadiness parameter *A* has significant effects on the velocity components and temperature profiles. The maximum axial velocity, transverse velocity and temperature profiles are attained when the flow is steady (*A* = 0).
- Increasing the values of the magnetic field strength decreases the momentum boundary layer thickness while increasing the thermal boundary layer thickness.
- The velocity components are enhanced as the Hall parameter increases.
- The fluid temperature increases with increasing values of thermal radiation as well as a heat source.
- The heat transfer rate and the skin friction coefficient in the *x*-direction are increased while the skin friction in the *z*-direction decreases as the unsteadiness parameter increases.
- The skin friction coefficients are enhanced while the heat transfer rate is depressed by increasing the values of magnetic strengths.

Competing interests
The authors declare that they do not have any conflict of interests in their submitted paper.

Authors' contributions
SS wrote the introduction, formulated the problem, generated and discussed the results and GTM wrote the code, generated and also discussed the results and proof read the manuscript. All authors read and approved the final manuscript.

Author details
[1]Department of Mathematics, University of Venda, Private Bag X5050, Thohoyandou, 0950, South Africa. [2]Department of Mathematics, University of Swaziland, Private Bag 4, Kwaluseni, Swaziland.

References
1. Sakiadis, BC: Boundary-layer behaviour on continuous solid surfaces: I. Boundary-layer equations for two-dimensional and axisymmetric flow. AIChE J. **7**, 26-28 (1961)
2. Sakiadis, BC: Boundary-layer behaviour on continuous solid surfaces: II. Boundary-layer equations for two-dimensional and axisymmetric flow. AIChE J. **7**, 221-225 (1961)
3. Shateyi, S, Motsa, SS: Hydromagnetic non-Darcy flow, heat and mass transfer over a stretching sheet in the presence of thermal radiation and ohmic dissipation. Can. J. Chem. Eng. **89**, 1388-1400 (2011)
4. Shateyi, S: Thermal radiation and buoyancy effects on heat and mass transfer over a semi-infinite stretching surface with suction and blowing. J. Appl. Math. **2008**, Article ID 414830 (2008). doi:10.1155/2008/414830
5. Singh, P, Jangid, A, Tomer, NS, Sinha, D: Effects of thermal radiation and magnetic field on unsteady stretching permeable sheet in presence of free stream velocity. Int. J. Inf. Math. Sci. **6**(3), 160-166 (2010)
6. Shateyi, S, Motsa, SS: Thermal radiation effects on heat and mass transfer over an unsteady stretching surface. Math. Probl. Eng. **2009**, Article ID 965603 (2009). doi:10.1155/2009/965603
7. Shateyi, S, Marewo, GT: A new numerical approach of MHD flow, heat and mass transfer for the UCM fluid over a stretching surface in the presence of thermal radiation. Math. Probl. Eng. **2013**, Article ID 670205 (2013). doi:10.1155/2013/670205
8. Jhankal, AK: Unsteady MHD boundary layer flow and heat transfer over a stretching surface. Int. J. Phys. Math. Sci. **3**(2), 110-114 (2013)
9. Pal, D, Mondal, H: Effects of temperature-dependent viscosity and variable thermal conductivity on MHD non-Darcy mixed convective diffusion of species over a stretching sheet. J. Egypt. Math. Soc. (2013). doi:10.1016/j.joems.2013.05.010
10. Pop, I, Watanabe, T: Hall effect on magnetohydrodynamic free convection about a semi-infinite vertical plate. Int. J. Eng. Sci. **32**, 1903-1911 (1994)
11. Abd El-Aziz, M: Flow and heat transfer over an unsteady stretching surface with Hall effect. Meccanica **45**, 97-109 (2010)
12. Shateyi, S, Motsa, SS: Variable viscosity on magnetohydrodynamic fluid flow and heat transfer over an unsteady stretching surface with Hall effect. Bound. Value Probl. **2010**, Article ID 257568 (2010). doi:10.1155/2010/257568
13. Pal, D: Hall current and MHD effects on heat transfer over an unsteady stretching permeable surface with thermal radiation. Comput. Math. Appl. **63**(7), 1161-1180 (2013)
14. Zaman, H: Hall effects on the unsteady incompressible MHD fluid flow with slip conditions and porous walls. Appl. Math. Phys. **1**(3), 31-38 (2013)
15. Ali, M, Alam, MS, Asaduzzaman: Hall effects on steady MHD boundary layer flow and heat transfer due to stretching plate in the presence of heat source or sink. Int. J. Sci. Eng. Res. **4**(8), 2178-2183 (2013)
16. Motsa, SS: A new spectral local linearization method for nonlinear boundary layer flow problems. J. Appl. Math. **2013**, Article ID 423628 (2013). doi:10.1155/2013/423628
17. Trefethen, LN: Spectral Methods in MATLAB. SIAM, Philadelphia (2000)
18. Motsa, SS, Shateyi, S: A successive linearization method approach to solving Lane-Emden type of equations. Math. Probl. Eng. **2012**, Article ID 280702 (2012). doi:10.1155/2012/280702
19. Motsa, SS, Shateyi, S: Successive linearization analysis of the effects of partial slip, thermal diffusion, and diffusion-thermo on steady MHD convective flow due to a rotating disk. Math. Probl. Eng. **2012**, Article ID 397637 (2012). doi:10.1155/2012/397637
20. Motsa, SS, Makinde, OD, Shateyi, S: Application of successive linearisation method to squeezing flow with bifurcation. Adv. Math. Phys. **2014**, Article ID 410620 (2014). doi:10.1155/2014/410620
21. Ishak, A, Nazar, R, Pop, I: Heat transfer over an unsteady stretching permeable surface with prescribed wall temperature. Nonlinear Anal., Real World Appl. **10**, 2909-2913 (2009)
22. Shateyi, S, Marewo, GT: On a new numerical approach for the laminar boundary layer flow and heat transfer along a stretching cylinder embedded in a porous medium with variable thermal conductivity. J. Appl. Math. **2013**, Article ID 576453 (2013). doi:10.1155/2013/576453